



Research paper

Development of highly potent phosphodiesterase 4 inhibitors with anti-neuroinflammation potential: Design, synthesis, and structure-activity relationship study of catecholamides bearing aromatic rings



Zhong-Zhen Zhou^{a,*}, Bing-Chen Ge^a, Qiu-Ping Zhong^a, Chang Huang^a, Yu-Fang Cheng^a,
Xue-Mei Yang^{b,**}, Hai-Tao Wang^a, Jiang-Ping Xu^{a,***}

^a Neuropharmacology Group, School of Pharmaceutical Sciences, Southern Medical University, Guangzhou 510515, China

^b Hygiene Detection Center, School of Public Health and Tropical Medicine, Southern Medical University, Guangzhou 510515, China

ARTICLE INFO

Article history:

Received 17 May 2016

Received in revised form

20 August 2016

Accepted 22 August 2016

Available online 24 August 2016

Keywords:

Catecholamides

Selective phosphodiesterase 4 inhibitors

Structure-activity relationship

Molecular docking

Anti-neuroinflammation activity

ABSTRACT

In this study, catecholamides (**7a–l**) bearing different aromatic rings (such as pyridine-2-yl, pyridine-3-yl, phenyl, and 2-chlorophenyl groups) were synthesized as potent phosphodiesterase (PDE) 4 inhibitors. The inhibitory activities of these compounds were evaluated against the core catalytic domains of human PDE4 (PDE4CAT), full-length PDE4A4, PDE4B1, PDE4C1, and PDE4D7 enzymes, and other PDE family members. Eight of the synthesized compounds were identified as having submicromolar IC₅₀ values in the mid-to low-nanomolar range. Careful analysis on the structure-activity relationship of compounds **7a–l** revealed that the replacement of the 4-methoxy group with the difluoromethoxy group improved inhibitory activities. More interesting, 4-difluoromethoxybenzamides **7i** and **7j** exhibited preference for PDE4 with higher selectivities of about 3333 and 1111-fold over other PDEs, respectively. In addition, compound **7j** with wonderful PDE4D7 inhibitory activities inhibited LPS-induced TNF- α production in microglia.

© 2016 Elsevier Masson SAS. All rights reserved.

1. Introduction

The enzymes collectively referred to as phosphodiesterase-4 (PDE-4) are bimetallic hydrolases that specifically catalyze the hydrolysis of second messenger cyclic adenosine monophosphate (cAMP), and are highly expressed in inflammatory and immune cell types, central nervous system (CNS) tissue, and smooth muscles of the lung [1–3]. The PDE4 family comprises 4 primary gene products (PDE4A–D), which are primarily found in inflammatory and immune cells, including T cells, B cells, macrophages, monocytes, neutrophils, and eosinophils. In fact, an increase in intracellular cAMP concentration, which results from the inhibition of PDE4, exerts a broad range of anti-inflammatory effects, anti-depressant-like effects, and long-term memory-enhancing effects.

Development of PDE4 inhibitors for anti-inflammatory therapy has been ongoing for several decades primarily targeted for the

treatment of asthma, chronic obstructive pulmonary disease (COPD), and atopic dermatitis (AD). Wide-spread use of the first-generation PDE4 inhibitors, such as rolipram (**1**), has been hampered by the occurrence of its mechanism-associated side effects, nausea and emesis, at effective doses. Second-generation selective inhibitors, roflumilast (**2**) [4], apremilast (**3**) [5], and cilomilast (**4**) [6], were generally better-tolerated; however, this was likely at dosages that did not achieve sustained PDE4 inhibition (Fig. 1). Although a large number of PDE4 inhibitors have been evaluated in the clinically, only roflumilast (**3**) [4] and apremilast (**4**) [5] are currently approved PDE4 inhibitors. Consequently, research efforts have shifted toward the selective PDE4 inhibitors in the hope that more selective inhibitors would have fewer side effects.

The catechol motif, which is known to accept a double hydrogen bond from the carboxamide of a glutamine residue at the back of the PDE4 catalytic site [7–9], is found in a range of PDE4 inhibitors, from the earliest described compounds such as rolipram to the currently marketed roflumilast and apremilast. In addition, many studies have indicated that an amide linker may be important for the selectivity. For example, roflumilast (**2**) and its *N*-oxide (**4**) with an amide linker display exceptional selectivity for PDE4 [10,11]. Our

* Corresponding author.

** Corresponding author.

*** Corresponding author.

E-mail addresses: zhouzz@smu.edu.cn (Z.-Z. Zhou), yxmjp@sina.com (X.-M. Yang), jpx@smu.edu.cn (J.-P. Xu).

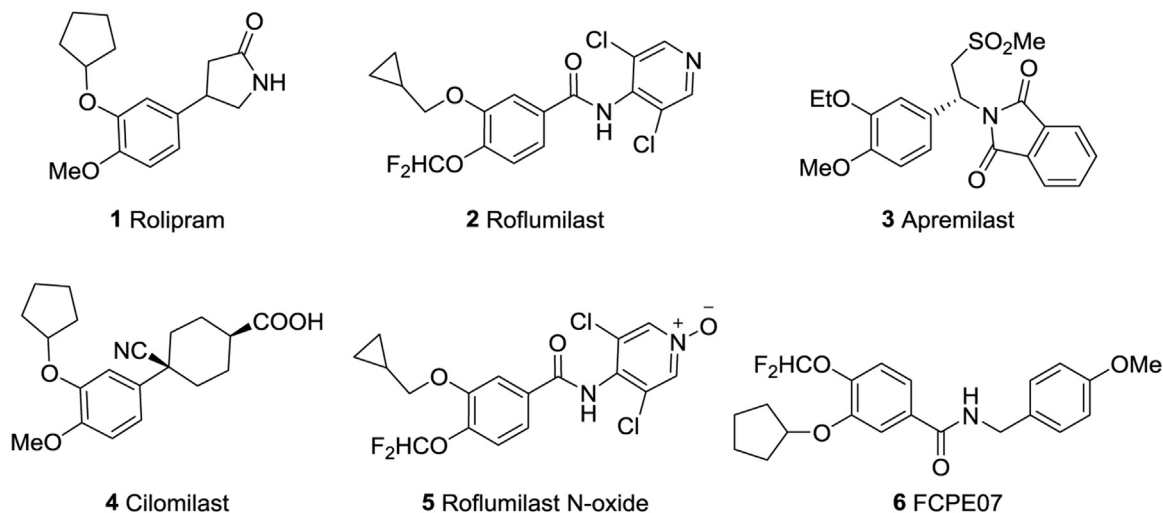


Fig. 1. PDE4 inhibitors.

recent research on selective PDE4 inhibitors led to the selective PDE4 inhibitor FCPE07 [12] which exhibited a 10-fold PDE4D7 selectivity over the PDE4B1 subtypes and an over 1000-fold selectivity against other PDE family members. To obtain more highly selective PDE4 inhibitors, we planned the synthesis of a series of *N*-arylbenzamides in this study by replacing the 4-methoxybenzyl group in the side chain of FCPE07 with other aromatic rings (such as pyridine-2-yl, pyridine-3-yl, phenyl, and 2-chlorophenyl, Fig. 2). The structure-activity relationships (SAR) of these compounds are also discussed.

2. Results and discussion

2.1. Chemistry

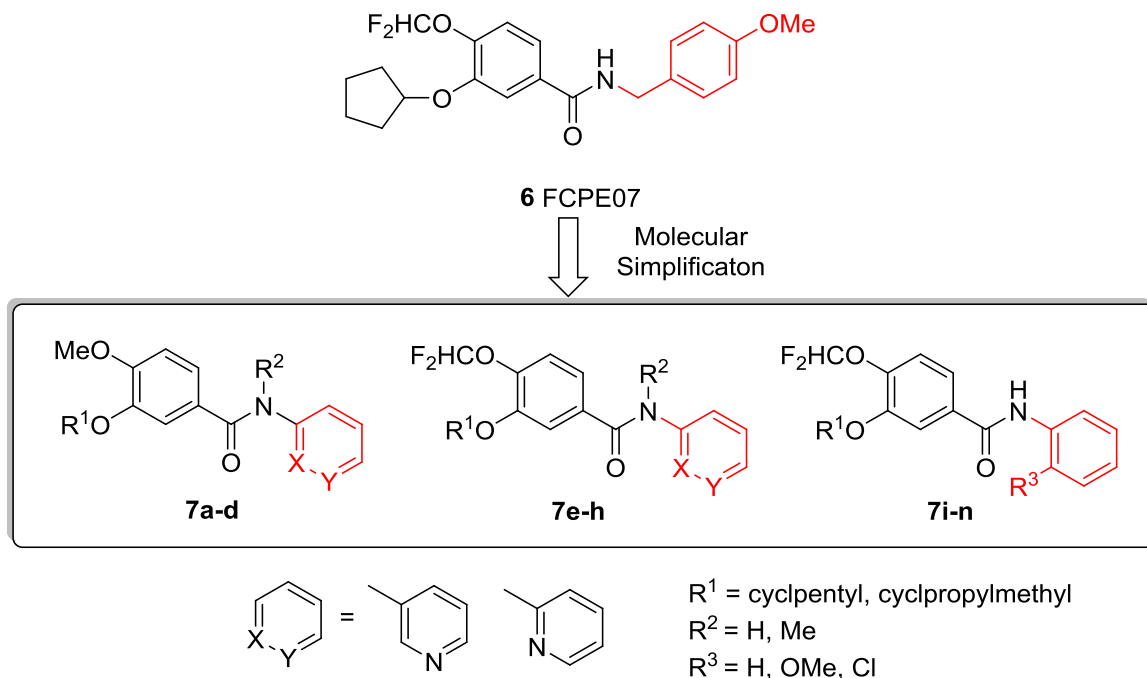
The target compounds **7a-l** were prepared from 3,4-dialkoxybenzoic acids (**8a-d**) using our prior synthetic

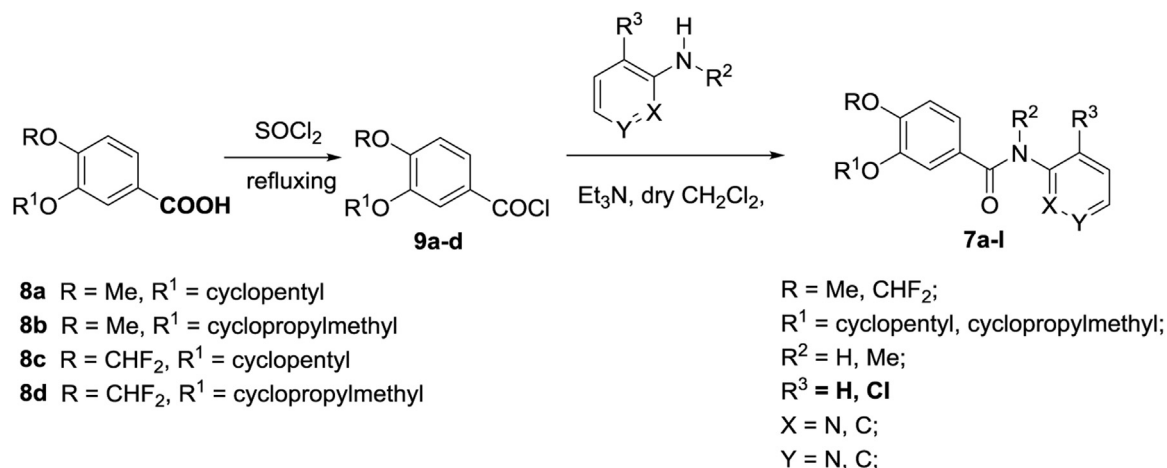
methodology [12], as shown in Scheme 1. Acids (**8a-d**) were converted by thionyl chloride to acid chlorides (**9a-d**), which were subsequently reacted with the corresponding amines to prepare benzamides **7a-l** in good yields.

2.2. Pharmacology

2.2.1. In vivo evaluation of compounds **7a-l**

Recent studies have indicated that the catalytic domains of all subtypes of PDE4 (PDE4A–D) exhibit a high degree of sequence conservation with a single active-site amino acid determining the nucleotide selectivity [10,13]. Preliminary tests on human PDE4CAT (the catalytic domains of PDE4, purchased from SB Drug Discovery) were performed as previously reported [14,15], using rolipram as a positive control. All compounds were tested on PDE4CAT at nine concentrations (10^{-8} – 10^{-4} M) and the IC_{50} values were determined by nonlinear regression analysis of their inhibition curves

Fig. 2. Design of *N*-arylbenzamides as selective PDE4 inhibitors.



Scheme 1. Synthetic route of compounds 7a-l.

(see Table 1). Among these compounds, most of the benzamides (**7a**, **7b**, **7e**, **7f**, **7i**, **7j**, **7k**, and **7l**) showed exceptional PDE4 inhibitory activities with the submicromolar IC₅₀ values in the mid-to low-nanomolar range, and up to 18-fold higher inhibitory activities than that of rolipram. Compound **7i** displayed the highest potency (IC₅₀ = 30 nM).

Careful analysis on the structure-activity relationship of compounds **7a-l** revealed that the replacement of the 4-methoxy group with the difluoromethoxy group improved inhibitory activities. For example, 4-difluoromethoxy compounds (**7e-h**) were about 2–10-fold more potent than the corresponding 4-methoxy substituted compounds (**7a-d**, Table 1). On the other hand, substitutions on the benzamide nitrogen had a profound impact on the activity. For example, *N*-(pyridine-3-yl)-benzamides (**7a**, **7b**, **7e**, and **7f**) displayed higher inhibitory activities than the corresponding *N*-methyl-*N*-(pyridin-2-yl)-benzamides (**7c**, **7d**, **7g**, and **7h**). Moreover, compounds **7i** and **7j** bearing a 2-chlorophenyl group showed higher activities than those of compounds **7k** and **7l**. The effects of the substituents on the benzamide nitrogen are as follows: 2-

Table 1
The inhibition of PDE4CAT.

Compound	R ¹	R ²		IC ₅₀ (nM) ^a
7a^b	cyclopentyl	H	Pyridine-3-yl	310
7b	cyclopropylmethyl	H	Pyridine-3-yl	360
7c	cyclopentyl	Me	Pyridine-2-yl	9700
7d	cyclopropylmethyl	Me	Pyridine-2-yl	25,100
7e	cyclopentyl	H	Pyridine-3-yl	140
7f	cyclopropylmethyl	H	Pyridine-3-yl	69
7g	cyclopentyl	Me	Pyridine-2-yl	1400
7h	cyclopropylmethyl	Me	Pyridine-2-yl	2500
7i	cyclopentyl	\	2-chlorophenyl	30
7j	cyclopropylmethyl	\	2-chlorophenyl	90
7k	cyclopentyl	\	phenyl	240
7l	cyclopropylmethyl	\	phenyl	220
Rolipram				550

^a Data reported are the mean of two experiments.

^b Compound **7a** has been previously reported [16].

chlorophenyl ≈ pyridin-3-yl > Phenyl > *N*-methyl-*N*-(pyridin-2-yl) [16].

In order to obtain the in vitro selectivity of compounds **7e**, **7f**, **7i**, and **7j** with best activities, these compounds were screened for human PDE1A, PDE2A, PDE3B, PDE4A4, PDE4B1, PDE4C1, PDE4D7, PDE5A, PDE6C, PDE7A, PDE8A1, PDE9A2, PDE10A2, and PDE11A, which were purchased from BPS Bioscience Inc. As shown in Table 2, compounds **7e** and **7f** bearing a pyridin-3-yl group displayed exceptional PDE4B1 and PDE4D7 inhibitory activities in the low-nanomolar range. Moreover, compounds **7i** and **7j** bearing a 2-chlorophenyl group exhibited some selectivity for PDE4D7, about 3- to 18-fold versus the other three PDE4 isoforms (PDE4A4, PDE4B1, and PDE4C1).

On the other hand, it is very clear that 4-difluoromethoxybenzamides (**7i** and **7j**) bearing a 2-chlorophenyl group on the benzamide nitrogen have more preference for PDE4 than the 4-difluoromethoxybenzamides (**7e** and **7f**) bearing a pyridine-2-yl group. For example, compounds **7i** and **7j** displayed a high selectivity for PDE4 over that of the other PDEs (PDE1-3 and PDE5-11), at least about 3333 and 1111-fold, respectively. However, compounds **7e** and **7f** showed low selectivity for PDE4 over PDE11A, although they showed good selectivity for PDE4 over PDE1A, PDE2A, PDE3B, PDE5A, PDE6C, PDE7A, PDE8A1, PDE9A2, and PDE10A2.

2.3. Molecular docking studies

In an effort to gain an understanding of the SARs observed, we studied the binding of the synthesized inhibitors with PDE4D using SYBYL 7.3. The crystal structure of human phosphodiesterase 4D with roflumilast was taken from a Protein Data Bank entry (PDB code 1XOQ) [10] and used as the starting point. The new inhibitors were built and optimized using the Powell method in SYBYL 7.3. Hydrogen and Gasteiger-Hückel charges were added to every molecule. Water molecules conserved in all PDE4D structures deposited into PDB were considered for the calculations.

Initially, we selected the most potent compounds **7f**, **7i** and **7j** for the docking experiments. The active site of the PDE4D catalytic domains is divided into three pockets [10]: the metal binding pocket (M), the purine-selective glutamine and hydrophobic clamp pocket (Q) (which is further divided into Q1 and Q2 subpockets), and the solvent-filled side pocket (S). As compared to roflumilast, compounds **7f**, **7i** and **7j** adopt the same conformations in the purine-selective glutamine and hydrophobic clamp pocket (Q1 and

Table 2

The inhibition of various PDEs by selected compounds.

PDEs	7e		7f		7i		7j		Rolipram
	1×10^4 nM ^a	IC ₅₀ (nM) ^b	1×10^4 nM ^a	IC ₅₀ (nM) ^b	1×10^4 nM ^a	IC ₅₀ (nM) ^b	1×10^4 nM ^a	IC ₅₀ (nM) ^b	IC ₅₀ (nM) ^b
PDE1A	0	$>1 \times 10^5$	20	$>1 \times 10^5$	3	$>1 \times 10^5$	6	$>1 \times 10^5$	NT ^c
PDE2A	26	$>1 \times 10^5$	23	$>1 \times 10^5$	28	$>1 \times 10^5$	8	$>1 \times 10^5$	NT ^c
PDE3B	6	$>1 \times 10^5$	6	$>1 \times 10^5$	6	$>1 \times 10^5$	13	$>1 \times 10^5$	NT ^c
PDE4CAT	98	140	98	69	98	30	96	90	550
PDE4A4	98	117	98	76	98	95	100	126	386
PDE4B1	99	39	99	34	100	144	98	166	86
PDE4C1	98	294	98	269	97	400	96	501	118
PDE4D7	99	68	100	71	99	22	99	39	160
PDE5A	12	$>1 \times 10^5$	23	$>1 \times 10^5$	7	$>1 \times 10^5$	12	$>1 \times 10^5$	NT ^c
PDE6C	16	$>1 \times 10^5$	28	$>1 \times 10^4$	2	$>1 \times 10^5$	2	$>1 \times 10^5$	NT ^c
PDE7A	3	$>1 \times 10^5$	7	$>1 \times 10^5$	3	$>1 \times 10^5$	7	$>1 \times 10^5$	NT ^c
PDE8A1	9	$>1 \times 10^5$	22	$>1 \times 10^5$	10	$>1 \times 10^5$	3	$>1 \times 10^5$	NT ^c
PDE9A2	4	$>1 \times 10^5$	8	$>1 \times 10^5$	6	$>1 \times 10^5$	3	$>1 \times 10^5$	NT ^c
PDE10A2	9	$>1 \times 10^5$	14	$>1 \times 10^5$	6	$>1 \times 10^5$	3	$>1 \times 10^5$	NT ^c
PDE11A	76	NT ^c	85	NT ^c	7	$>1 \times 10^5$	5	$>1 \times 10^5$	NT ^c

^a Inhibition (%) at 1×10^4 nM. Data reported are the mean of two experiments.^b Data reported are the mean of two experiments.^c NT = not tested.

Q2) with subtle apparent variances (Fig. 3). In the active site of PDE4 catalytic domains, the difluoromethoxy group and the cyclopropylmethoxy or cyclopentylmethoxy group bind at the purine-selective glutamine and hydrophobic clamp pocket, while the difluoromethyl group is in a position to form a hydrogen bond with the N–H of Asn321. Thus, as compared to compounds (**7a–d**) bearing a 4-methoxy group, the improvement in activity of compounds (**7e–h**) bearing a 4-difluoromethoxy group could be

attributed to the extra H-bond of the 4-difluoromethyl group with the residue Asn487.

In the binding mode of roflumilast, the amide linker is in a position to form a hydrogen bond with a conserved water molecule, which extends to Zn^{2+} , whereas the dichloropyridyl group extends to the bimetallic ion site and forms one H bond with a water molecule that is coordinated to Mg^{2+} . In contrast to the binding mode of roflumilast, the pyridyl group in compound **7f** (Fig. 3B)

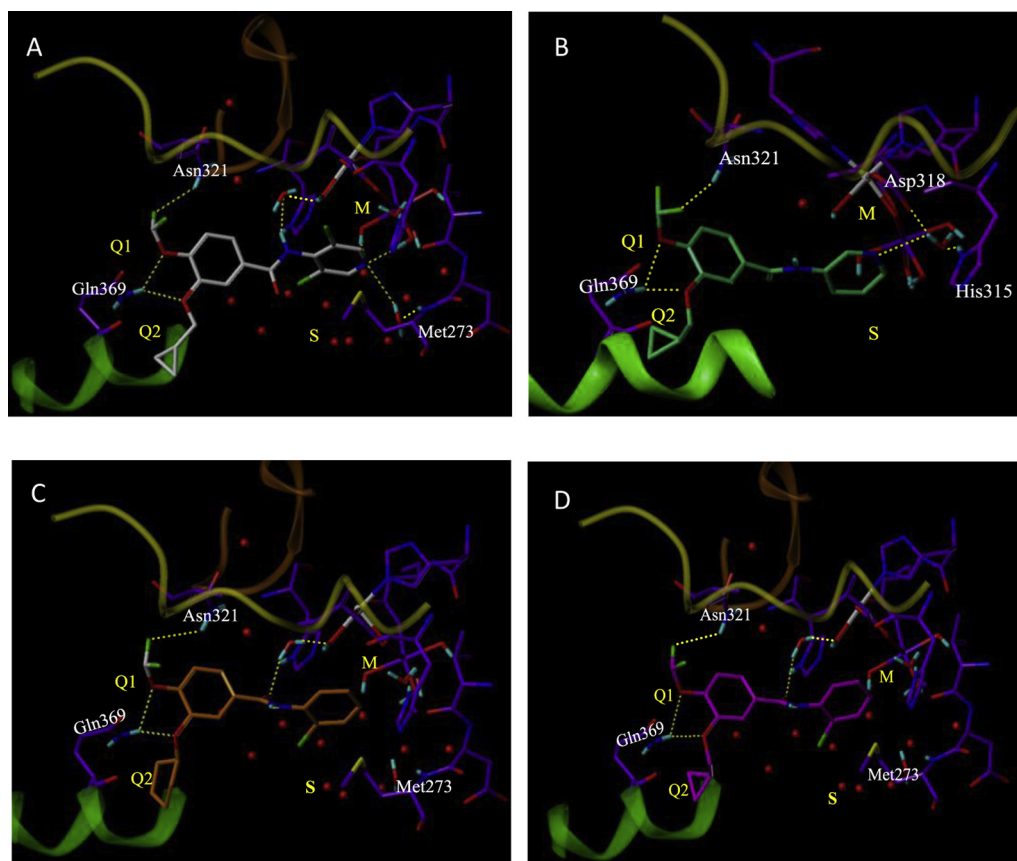


Fig. 3. Binding mode of roflumilast (A), **7f** (B), **7i** (C) and **7j** (D) in the catalytic pocket of PDE4D. The H-bonds are shown in yellow. C atoms of roflumilast, **7f**, **7i** and **7j** are colored in white, green-blue, orange, and violet respectively. (For interpretation of the references to colour in this figure legend, the reader is referred to the web version of this article.)

forms a hydrogen bond with a conserved water molecule in the M pocket, which leads to the amide linker having no intermolecular hydrogen bond. In the binding mode of compound **7i** (Fig. 3C) and **7j** (Fig. 3D), the amide linker is also in position to form a hydrogen bond with a conserved water molecule, which extends to Zn²⁺. Compound **7i** and **7j** displayed selectivity for PDE4 over other PDEs (PDE1–3 and PDE5–11). However, compound **7f** showed good inhibitory activity toward PDE11A at the concentration of 10 μM. This suggests that the hydrogen bond of the amide linker with conserved water may be important to the PDE4 selectivity.

2.4. Anti-neuroinflammation activity in microglial cells

Evidence suggests that chronic low-grade inflammation plays an important role in the pathology of depression [17,18]. Pro-inflammatory cytokines and acute phase proteins, which normally coordinate the local and systemic inflammatory response to microbial pathogens, also appear to act directly on the brain, where they cause behavioral symptoms, including sickness [19]. PDE4 regulates the pro-inflammatory toll receptor–TNF-α pathway in monocytes, macrophages and microglial cells (BV-2) [20]. Thus, western blotting analysis was used to assess the protein levels of PDE4 inhibitor **7j** (5, 20, 80 μM, final DMSO concentration = 5%), and TNF-α response to explore the neurochemical mechanisms (Fig. 4).

To investigate the effects of compounds **7j** on pro-inflammatory cytokine production, microglial cells were treated with different concentrations of **7j** for 1 h, and then incubated with LPS (1 μg/ml) for 24 h. As shown in Fig. 4, compounds **7j** alone had no effect on the production of TNF-α in the microglia at 80 μM. Stimulation of microglia with LPS alone led to a significant increase in the TNF-α levels after 24 h. Compound **7j** significantly suppressed LPS-induced increase of TNF-α production in a concentration-dependent manner (Fig. 4). These data demonstrated that compound **7j** inhibited LPS-induced TNF-α production in microglia ($p < 0.01$) at the concentration of 80 μM. Further, microglia cells treated with **7j** at the concentration of 5 μM also inhibited LPS-induced TNF-α production.

3. Conclusion

In conclusion, catecholamides were designed and synthesized as potential PDE4 inhibitors. Among these compounds, most of the

benzamides (compounds **7a**, **7b**, **7e**, **7f**, **7i**, **7j**, **7k**, and **7l**) showed exceptional PDE4 inhibitory activities. More interestingly, 4-difluoromethoxybenzamides (**7i** and **7j**) bearing a 2-chlorophenyl group on the benzamide nitrogen have more preference for PDE4, at least about 3333 and 1111-fold selectivity for PDE4 over other PDEs (PDE1–3 and PDE5–11). Moreover, compound **7j** inhibited LPS-induced TNF-α production in microglia.

In the PDE4D catalytic domain, docking studies revealed that the compounds **7f**, **7i** and **7j** adopt the same conformations in the purine-selective glutamine and hydrophobic clamp pocket (Q1 and Q2), with subtle apparent variances, and the difluoromethyl group is in a position to form a hydrogen bond with the N-H of Asn321. In addition, the amide linker of roflumilast and compound **7i** and **7j** is in a position to form a hydrogen bond with a conserved water molecule, which extends to Zn²⁺, but the amide linker of **7f** has no hydrogen bond with the others. Further efforts will be aimed at developing more potent PDE4 inhibitors with increased activity and selectivity.

4. Experimental section

4.1. Chemistry

Melting points were determined in open glass capillaries using an X-5 apparatus and are uncorrected. ESI-MS spectra were measured on a Waters UPLC/Quattro Premier XE mass spectrometer. ¹H and ¹³C NMR spectra were recorded in CDCl₃ or DMSO-*d*₆ using a Varian Mercury 400 spectrometer and TMS as an internal reference. Elemental analyses were carried out on a Vario ELIII CHNSO elemental analyzer. Rolipram was purchased from Sigma (St. Louis, MO, USA). All the other chemicals were of analytical grade and used without further purification.

4.1.1. General procedure for the synthesis of compounds **7a–l**

To the intermediate alkoxybenzoic acid (0.5 mmol), excess thionyl chloride (5 mL) was added, and the reaction mixture was stirred at 60–80 °C for 3 h. The excess thionyl chloride was evaporated under reduced pressure to give corresponding alkoxybenzoyl chloride (**9a–d**) as crude yellow oil, which was used in all the following reactions without further purification.

Suitable amine (0.5 mmol) and anhydrous triethylamine (1 mmol) were dissolved in dry CH₂Cl₂ (5 mL). The mixture was cooled on ice and treated dropwise (during 5 min) with a solution of previously prepared alkoxybenzoyl chloride in dry CH₂Cl₂ (2 mL) at 0 °C. The reaction mixture was stirred at room temperature for 3 h and monitored by TLC. Then, the reaction mixture was concentrated under reduced pressure and the obtained residue was chromatographed using a mixture of petroleum ether and acetone (v/v = 20:1) to give target compounds.

All new compounds were fully characterized by MS and NMR (¹H and ¹³C) (see Supporting Information).

4.1.1.1. N-(pyridin-3-yl)-3-cyclopropylmethoxy-4-methoxybenzamide (7b). Yield: 39%. ¹H NMR (400 MHz, CDCl₃) δ 9.34 (s, 1H), 9.21 (d, *J* = 2.3 Hz, 1H), 8.86–8.79 (m, 1H), 8.30 (dd, *J* = 5.2, 1.2 Hz, 1H), 7.70 (dd, *J* = 8.4, 2.1 Hz, 1H), 7.60 (d, *J* = 2.1 Hz, 1H), 7.52 (dd, *J* = 8.5, 5.1 Hz, 1H), 6.93 (d, *J* = 8.5 Hz, 1H), 3.96 (d, *J* = 7.0 Hz, 2H), 3.93 (s, 3H), 1.38–1.31 (m, 1H), 0.68–0.61 (m, 2H), 0.39–0.33 (m, 2H). ¹³C NMR (100 MHz, CDCl₃) δ 166.1, 152.9, 148.6, 142.3, 139.7, 136.6, 129.5, 126.1, 124.4, 120.7, 112.6, 110.7, 74.2, 56.1, 10.2, 3.5. ESI-MS (*m/z*): 321.8 ([M+Na]⁺), 299.8 ([M+H]⁺). and Anal. Calcd. for C₁₇H₁₈N₂O₃: C, 68.44; H, 6.08; N, 9.39; Found: C, 68.13; H, 5.89; N, 9.07.

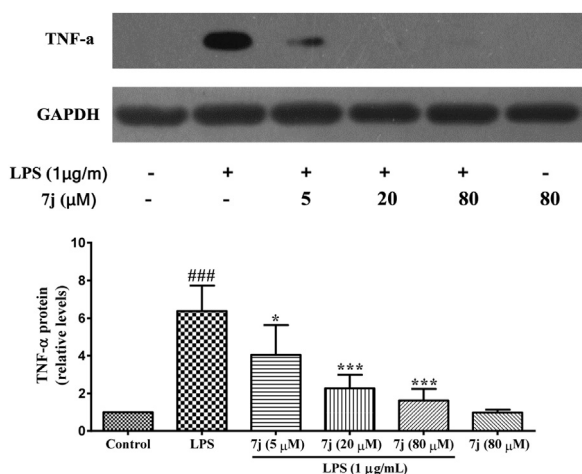


Fig. 4. Compounds **7j** inhibited LPS-induced production of pro-inflammatory cytokines in microglial cells. Data are expressed as mean ± SEM ($n = 3$ /group). ### $p < 0.001$, * $p < 0.01$, *** $p < 0.001$, compared to the control group.

4.1.1.2. N-methyl-N-(pyridin-2-yl)-3-cyclopentyl-4-methoxybenzamide (7c). Yield: 57%. ^1H NMR (400 MHz, CDCl_3) δ 8.48 (dd, $J = 4.8, 1.2$ Hz, 1H), 7.51–7.46 (m, 1H), 7.08–7.05 (m, 1H), 7.01 (dd, $J = 8.4, 2.0$ Hz, 1H), 6.86 (d, $J = 2.0$ Hz, 1H), 6.81 (d, $J = 8.0$ Hz, 1H), 6.71 (d, $J = 8.4$ Hz, 1H), 4.56–4.51 (m, 1H), 3.81 (s, 3H), 3.61 (s, 3H), 1.85–1.66 (m, 6H), 1.59–1.53 (m, 2H). ^{13}C NMR (100 MHz, CDCl_3) δ 170.8, 157.4, 151.8, 148.6, 146.8, 137.4, 127.9, 122.3, 121.8, 120.6, 115.3, 110.8, 80.3, 55.9, 36.1, 32.7. ESI-MS (m/z): 349.9. ($[\text{M}+\text{Na}]^+$), 327.9 ($[\text{M}+\text{H}]^+$). and Anal. Calcd. for $\text{C}_{19}\text{H}_{22}\text{N}_2\text{O}_3$: C, 69.92; H, 6.79; N, 8.58; Found: C, 70.11; H, 6.90; N, 8.35.

4.1.1.3. N-methyl-N-(pyridin-2-yl)-3-cyclopropylmethoxy-4-methoxybenzamide (7d). Yield: 44%. ^1H NMR (400 MHz, CDCl_3) δ 8.47 (d, $J = 4.8$ Hz, 1H), 7.47 (t, $J = 7.8$ Hz, 1H), 7.10–7.04 (m, 1H), 6.94 (d, $J = 8.4$ Hz, 1H), 6.90 (s, 1H), 6.80 (d, $J = 8.0$ Hz, 1H), 6.69 (d, $J = 8.0$ Hz, 1H), 3.84 (s, 3H), 3.66 (d, $J = 7.2$ Hz, 2H), 3.60 (s, 3H), 1.23–1.15 (m, 1H), 0.62–0.58 (m, 2H), 0.31–0.27 (m, 2H). ^{13}C NMR (100 MHz, CDCl_3) δ 170.6, 157.1, 151.4, 148.0, 147.8, 138.0, 127.7, 122.6, 121.9, 120.6, 113.8, 110.5, 73.9, 55.9, 36.3, 10.1, 3.4. ESI-MS (m/z): 335.6. ($[\text{M}+\text{Na}]^+$), 313.6 ($[\text{M}+\text{H}]^+$). and Anal. Calcd. for $\text{C}_{18}\text{H}_{20}\text{N}_2\text{O}_3$: C, 69.21; H, 6.45; N, 8.97; Found: C, 69.49; H, 6.59; N, 9.25.

4.1.1.4. N-(pyridin-3-yl)-3-cyclopentyl-4-difluoromethoxybenzamide (7e). Yield: 51%. ^1H NMR (400 MHz, CDCl_3) δ 9.40 (s, 1H), 9.25 (d, $J = 2.0$ Hz, 1H), 8.84 (d, $J = 8.4$ Hz, 1H), 8.34 (dd, $J = 5.2, 0.8$ Hz, 1H), 7.70 (d, $J = 2.0$ Hz, 1H), 7.61 (dd, $J = 8.4, 2.0$ Hz, 1H), 7.57–7.52 (m, 1H), 7.23 (d, $J = 8.4$ Hz, 1H), 6.63 (t, $J = 74.8$ Hz, 1H, $-\text{CHF}_2$), 5.01–4.97 (m, 1H), 1.99–1.76 (m, 6H), 1.70–1.61 (m, 2H). ^{13}C NMR (100 MHz, CDCl_3) δ 165.6, 149.9, 144.0, 143.1, 140.0 (t, $J = 3.1$ Hz), 136.1, 132.0, 129.4, 124.4, 122.4, 119.2, 118.5 ($-\text{CHF}_2$), 115.9 ($-\text{CHF}_2$), 114.9, 113.3 ($-\text{CHF}_2$), 81.1, 32.7, 23.9. ESI-MS (m/z): 371.4 ($[\text{M}+\text{Na}]^+$), 349.5 ($[\text{M}+\text{H}]^+$). and Anal. Calcd. for $\text{C}_{18}\text{H}_{18}\text{F}_2\text{N}_2\text{O}_3$: C, 62.06; H, 5.21; N, 8.04; Found: C, 62.31; H, 5.31; N, 8.39.

4.1.1.5. N-(pyridin-3-yl)-3-cyclopropylmethoxy-4-difluoromethoxybenzamide (7f). Yield: 60%. ^1H NMR (400 MHz, CDCl_3) δ 8.86 (d, $J = 2.4$ Hz, 1H), 8.53 (s, 1H), 8.44 (d, $J = 8.4$ Hz, 1H), 8.37 (d, $J = 4.8$ Hz, 1H), 7.60 (d, $J = 1.6$ Hz, 1H), 7.46 (dd, $J = 8.2, 1.8$ Hz, 1H), 7.40 (dd, $J = 8.4, 4.8$ Hz, 1H), 7.24 (d, $J = 8.4$ Hz, 1H), 6.73 (t, $J = 74.8$ Hz, 1H), 3.96 (d, $J = 6.8$ Hz, 2H), 1.34–1.28 (m, 1H), 0.68–0.64 (m, 2H), 0.38–0.34 (m, 2H). ^{13}C NMR (100 MHz, CDCl_3) δ 165.5, 150.7, 143.9, 140.6, 135.7, 132.1, 128.9, 124.3, 122.0, 119.6, 118.4 ($-\text{CHF}_2$), 115.8 ($-\text{CHF}_2$), 114.0, 114.0, 113.2 ($-\text{CHF}_2$), 74.2, 10.0, 3.26. ESI-MS (m/z): 357.5 ($[\text{M}+\text{Na}]^+$), 335.5 ($[\text{M}+\text{H}]^+$) and Anal. Calcd. for $\text{C}_{17}\text{H}_{16}\text{F}_2\text{N}_2\text{O}_3$: C, 61.07; H, 4.82; N, 8.38; Found: C, 61.30; H, 4.97; N, 8.59.

4.1.1.6. N-methyl-N-(pyridin-2-yl)-3-cyclopentyl-4-difluoromethoxybenzamide (7g). Yield: 73%. ^1H NMR (400 MHz, CDCl_3) δ 8.48 (dd, $J = 5.0, 1.4$ Hz, 1H), 7.57–7.11 (m, 1H), 7.14–7.11 (m, 1H), 7.00 (d, $J = 8.4$ Hz, 1H), 6.97 (d, $J = 1.6$ Hz, 1H), 6.92 (dd, $J = 8.0, 2.0$ Hz, 1H), 6.87 (d, $J = 8.4$ Hz, 1H), 6.50 (t, $J = 75.2$ Hz, 1H, $-\text{CHF}_2$), 4.65–4.58 (m, 1H), 3.61 (s, 3H), 1.84–1.66 (m, 6H), 1.64–1.55 (m, 2H). ^{13}C NMR (100 MHz, CDCl_3) δ 169.9, 156.7, 149.0, 148.7, 142.2 (t, $J = 3.1$ Hz), 137.9, 134.0, 122.1, 121.6, 121.4, 121.2, 118.6 ($-\text{CHF}_2$), 116.0 ($-\text{CHF}_2$), 115.6, 113.4 ($-\text{CHF}_2$), 80.7, 36.2, 32.6, 23.8. ESI-MS (m/z): 385.5 ($[\text{M}+\text{Na}]^+$), 363.5 ($[\text{M}+\text{H}]^+$). and Anal. Calcd. for $\text{C}_{19}\text{H}_{20}\text{F}_2\text{N}_2\text{O}_3$: C, 62.98; H, 5.56; N, 7.73; Found: C, 62.69; H, 5.31; N, 7.61.

4.1.1.7. N-methyl-N-(pyridin-2-yl)-3-cyclopropylmethoxy-4-difluoromethoxybenzamide (7h). Yield: 83%. ^1H NMR (400 MHz,

CDCl_3) δ 8.45 (dd, $J = 4.8, 1.2$ Hz, 1H), 7.52–7.47 (m, 1H), 7.10–7.06 (m, 1H), 7.00–6.96 (m, 2H), 6.87–6.78 (m, 2H), 6.59 (t, $J = 75.0$ Hz, 1H), 3.71 (d, $J = 6.8$ Hz, 2H), 3.57 (s, 3H), 1.18–1.14 (m, 1H), 0.63–0.58 (m, 2H), 0.31–0.27 (m, 2H). ^{13}C NMR (100 MHz, CDCl_3) δ 169.8, 156.8, 149.9, 148.7, 141.7 (t, $J = 3.1$ Hz), 137.8, 134.1, 121.7, 121.6, 121.2, 118.5 ($-\text{CHF}_2$), 115.9 ($-\text{CHF}_2$), 114.9, 113.3 ($-\text{CHF}_2$), 73.9, 36.2, 9.9, 3.2. ESI-MS (m/z): 371.5 ($[\text{M}+\text{Na}]^+$), 349.5 ($[\text{M}+\text{H}]^+$). and Anal. Calcd. for $\text{C}_{18}\text{H}_{18}\text{F}_2\text{N}_2\text{O}_3$: C, 62.06; H, 5.21; N, 8.04; Found: C, 61.87; H, 5.33; N, 8.23.

4.1.1.8. N-(2-chlorophenyl)-3-cyclopentyl-4-difluoromethoxybenzamide (7i). Yield: 45%. ^1H NMR (400 MHz, CDCl_3) δ 8.53 (dd, $J = 8.3, 1.6$ Hz, 1H), 8.40 (s, 1H), 7.60 (d, $J = 2.0$ Hz, 1H), 7.12–7.01 (m, 1H), 7.40–7.32 (m, 2H), 7.27–7.24 (m, 2H), 7.11–7.07 (m, 1H), 6.63 (t, $J = 75.0$ Hz, 1H), 4.95–4.90 (m, 1H), 2.04–1.77 (m, 6H), 1.71–1.62 (m, 2H). ^{13}C NMR (100 MHz, CDCl_3) δ 164.4, 150.1, 143.8, 134.6, 132.9, 129.1, 127.9, 124.9, 123.0, 122.7, 121.4, 118.6, 118.5 ($-\text{CHF}_2$), 115.9 ($-\text{CHF}_2$), 114.6, 113.3 ($-\text{CHF}_2$), 81.0, 32.8, 23.9. Negative ESI-MS (m/z): 380.4 ($[\text{M}-\text{H}]^-$). and Anal. Calcd. for $\text{C}_{19}\text{H}_{18}\text{ClF}_2\text{NO}_3$: C, 59.77; H, 4.75; N, 3.67; Found: C, 59.51; H, 4.90; N, 3.49.

4.1.1.9. N-(2-chlorophenyl)-3-cyclopropylmethoxy-4-difluoromethoxybenzamide (7j). Yield: 46%. ^1H NMR (400 MHz, CDCl_3) δ 8.52 (dd, $J = 8.2, 1.4$ Hz, 1H), 8.39 (s, 1H), 7.59 (d, $J = 2.0$ Hz, 1H), 7.45–7.31 (m, 3H), 7.30–7.26 (m, 2H), 7.13–7.06 (m, 1H), 6.73 (t, $J = 75.0$ Hz, 1H), 3.98 (d, $J = 6.9$ Hz, 2H), 1.38–1.29 (m, 1H), 0.73–0.62 (m, 2H), 0.43–0.33 (m, 2H). ^{13}C NMR (100 MHz, CDCl_3) δ 164.3, 150.9, 143.3, 134.6, 133.0, 129.1, 127.9, 124.9, 123.1, 122.3, 121.5, 118.9, 118.4 ($-\text{CHF}_2$), 115.8 ($-\text{CHF}_2$), 113.9, 113.2 ($-\text{CHF}_2$), 74.2, 10.0, 3.3. ESI-MS (m/z): 390.6 ($[\text{M}+\text{Na}]^+$). and Anal. Calcd. for $\text{C}_{18}\text{H}_{16}\text{ClF}_2\text{NO}_3$: C, 58.78; H, 4.39; N, 3.81; Found: C, 58.59; H, 4.17; N, 3.62.

4.1.1.10. N-phenyl-3-cyclopentyl-4-difluoromethoxybenzamide (7k). Yield: 86%. ^1H NMR (400 MHz, CDCl_3) δ 7.79 (s, 1H), 7.67–7.59 (m, 2H), 7.56 (d, $J = 2.0$ Hz, 1H), 7.41–7.34 (m, 2H), 7.30 (dd, $J = 8.2, 2.0$ Hz, 1H), 7.23–7.13 (m, 2H), 6.61 (t, $J = 75.1$ Hz, 1H), 4.93–4.86 (m, 1H), 2.00–1.77 (m, 6H), 1.70–1.62 (m, 2H). ^{13}C NMR (100 MHz, CDCl_3) δ 164.9, 150.0, 143.5, 137.8, 133.3, 129.1, 124.8, 122.4, 120.3, 118.5 ($-\text{CHF}_2$), 118.3, 115.9 ($-\text{CHF}_2$), 114.7, 113.3 ($-\text{CHF}_2$), 81.0, 32.7, 23.9. Negative ESI-MS (m/z): 346.5 ($[\text{M}-\text{H}]^-$). and Anal. Calcd. for $\text{C}_{19}\text{H}_{19}\text{F}_2\text{NO}_3$: C, 65.70; H, 5.51; N, 4.03; Found: C, 65.39; H, 5.27; N, 3.96.

4.1.1.11. N-phenyl-3-cyclopropylmethoxy-4-difluoromethoxybenzamide (7l). Yield: 82%. ^1H NMR (400 MHz, CDCl_3) δ 7.80 (s, 1H), 7.67–7.59 (m, 2H), 7.54 (d, $J = 1.6$ Hz, 1H), 7.42–7.30 (m, 3H), 7.25–7.13 (m, 2H), 6.71 (t, $J = 75.1$ Hz, 1H), 3.94 (d, $J = 6.9$ Hz, 2H), 1.37–1.29 (m, 1H), 0.70–0.60 (m, 2H), 0.41–0.30 (m, 2H). ^{13}C NMR (100 MHz, CDCl_3) δ 164.8, 150.8, 143.0, 137.7, 133.3, 129.1, 124.8, 122.2, 120.3, 118.8, 118.4 ($-\text{CHF}_2$), 115.8 ($-\text{CHF}_2$), 113.9, 113.2 ($-\text{CHF}_2$), 74.1, 10.0, 3.3. Negative ESI-MS (m/z): 332.5 ($[\text{M}-\text{H}]^-$). and Anal. Calcd. for $\text{C}_{18}\text{H}_{17}\text{F}_2\text{NO}_3$: C, 64.86; H, 5.14; N, 4.20; Found: C, 64.58; H, 5.03; N, 4.37.

4.2. Pharmacology

4.2.1. Materials

Compounds **7a–l** were dissolved in DMSO and stored as stock solutions (100 mM) at -20°C . For experimental use, all the compounds were prepared from stock solutions, diluted with growth medium and used immediately. FAM-Cyclic-3',5' -AMP and IMAP binding reagent IMAP binding reagent were purchased from Molecular Devices Inc. PDE4CAT and Other PDEs were purchased from

Sbdrugdiscovery Inc. and BPS Bioscience Inc. respectively.

4.2.2. In vitro assay of compounds for the inhibition of PDEs

A standard PDE assay was conducted. All of our assays used a substrate concentration below the K_m we determined for each enzyme such that $K_i = IC_{50}$. Our assay utilized IMAP technology (Molecular Devices), which is based on the high-affinity binding of phosphate by immobilized metal coordination complexes on nanoparticles. The binding reagent complexes with phosphate groups on nucleotide mono-phosphate generated from cyclic nucleotides (cAMP/cGMP) through PDEs. With detection by fluorescence polarization, binding causes a change in the rate of the molecular motion of the phosphate-bearing molecule and results in an increase in the fluorescence polarization value observed for the fluorescent label attached to the substrate.

These assays were carried out as described previously [14]. All of the enzymatic reactions were conducted at 25 °C for 60 min. The 50 μ l reaction mixture contains 40 mM MOPS, pH 7.5, 0.5 mM EDTA, 15 mM $MgCl_2$, 0.15 mg/ml BSA, 1 mM DTT, 0.05% Proclin 200, 15 ng/ml PDE 4CAT and 100 nM FAM-Cyclic-3',5'-AMP. The compounds were diluted in 10% DMSO and 5 μ l of the dilution was added to a 50 μ l reaction so that the final concentration of DMSO is 1% in all of reactions. The reaction mixture was incubated at 25 °C for 1 h. Then add 100 μ l diluted binding agent to each well and incubate at 25 °C for 1 h with slow shaking. Read the fluorescence polarization of the sample used an excitation filter of 360 nm and an emission filter of 480 nm.

The percentage of inhibition was calculated using the following formula: % activity = $[(FP_{drug} - FP_{control}) / (FP_{enzyme} - FP_{control})] \times 100\%$. The IC_{50} values were calculated using nonlinear regression with normalized dose–response fit using Prism GraphPad software.

4.3. Molecular docking

Molecular docking was performed with Surflex-Dock program that is interfaced with Sybyl 7.3. The programs adapted an empirical scoring function and a patented searching engine [21,22]. Ligand was docked into the corresponding protein's binding site guided by protomol, which is an idealized representation of a ligand that makes every potential interaction with binding site. In this work, the protomol was established by ligand from the crystal structure of PDE4D (PDB entry: 1XOQ) [10]. Beginning of docking, all ligands were removed and the random hydrogen atoms were added. Then the receptor structure was minimized in 10,000 cycles with Powell method in sybyl 7.3. All the compounds were constructed using sketch molecular module. Hydrogen and Gasteiger-Hückel charges were added to every molecular. Then their geometries are optimized by conjugate gradient method in TRIPOS force field. The energy convergence criterion is 0.001 kcal/mol. Default values were chosen to finish this work except that the threshold was 1 when the protomol was generated.

In order to validate the docking reliability, the ligand roflumilast was removed from the active site and docked back into the binding pocket. The root mean square deviation (RMSD) between the predicted conformation and the actual conformation from the crystal structure of ligand was 0.60 Å, which is smaller than the resolution of X-ray crystallography (1.83 Å) [10]. Its mean that the parameters set for this Surflex-dock simulation could successfully reproduce the ligand-binding motif from the X-ray structure, and could be extended to predict binding conformations of the synthesized inhibitors.

4.4. Western blot analysis

Cell Culture BV-2 cell line was maintained in DMEM supplemented with 10% heat-inactivated fetal bovine serum, 100 IU/mL penicillin and 100 μ g/mL streptomycin at 37 °C in a humidified 5% CO_2 incubator.

Each protein sample were separated by using 12% sodium dodecyl sulphate polyacrylamide gel electrophoresis (SDS-PAGE), transferred to polyvinylidene difluoride membrane (PVDF) and blocked by incubation with 5% non-fat milk for 2 h at room temperature. Following blotting, membranes were incubated with primary antibodies (anti-TNF- α , MILLIPORE, ab1837p; anti-GAPDH, abcam, ab181602) at 4 °C overnight, washed five times and incubated with secondary antibodies (Peroxidase Conjugated Goat anti-Rabbit IgG (h+I), Fdbio science, FDR007) for 4 h at 4 °C. Membranes were then detected by enhanced chemiluminescence (ECL), visualized using a Kodak Digital Science ID, and quantified with ImageJ software 6.0.

Acknowledgments

This work was financially supported by Foundation for Guangdong Distinguished Young Teachers in Higher Education of China (No. C1032190), and Science and Technology Program of Guangdong Province of China (No. 2016A020217008) awarded to Z.Z.Z., and the National Science and Technology Major Projects of China for “Major New Drug Innovation and Development” (No. 2012ZX09J1211003C), NSFC-Guangdong Joint Fund (No. U1032006), and the National Natural Science Foundation of China (No. 81373384) awarded to J. P. X.

Appendix A. Supplementary data

Supplementary data related to this article can be found at <http://dx.doi.org/10.1016/j.ejmech.2016.08.052>.

References

- [1] A. Gavaldà, R.S. Roberts, Phosphodiesterase-4 inhibitors: a review of current developments (2010–2012), *Expert Opin. Ther. Pat.* 23 (2013) 997–1016.
- [2] A. Kodimuthali, S.S.L. Jabaris, M. Pal, Recent advances on phosphodiesterase 4 inhibitors for the treatment of asthma and chronic obstructive pulmonary disease, *J. Med. Chem.* 51 (2008) 5471–5489.
- [3] A. Garcia-Osta, M. Cuadrado-Tejedor, C. Garcia-Barroso, J. Oyarzabal, R. Franco, Phosphodiesterases as therapeutic targets for Alzheimer's disease, *ACS Chem. Neurosci.* 3 (2012) 832–844.
- [4] D.P. Tashkin, Roflumilast: the new orally active, selective phosphodiesterase-4 inhibitor, for the treatment of COPD, *Expert Opin. Pharmacother.* 15 (2014) 85–96.
- [5] H. Abdulrahim, S. Thistleton, A.O. Adebajo, T. Shaw, C. Edwards, A. Wells, Apremilast: a PDE4 inhibitor for the treatment of psoriatic arthritis, *Expert Opin. Pharmacother.* 16 (2015) 1099–1108.
- [6] D. Spina, PDE4 inhibitors: current status, *Br. J. Pharmacol.* 155 (2008) 308–315.
- [7] G.-F. Yang, H.-T. Lu, Y. Xiong, C.-G. Zhan, Understanding the structure–activity and structure–selectivity correlation of cyclic guanine derivatives as phosphodiesterase-5 inhibitors by molecular docking, CoMFA and CoMSIA analyses, *Bioorg. Med. Chem.* 14 (2006) 1462–1473.
- [8] Y. Xiong, H.-T. Lu, Y. Li, G.-F. Yang, C.-G. Zhan, Characterization of a Catalytic ligand bridging metal ions in phosphodiesterases 4 and 5 by molecular dynamics simulations and hybrid quantum mechanical/molecular mechanical calculations, *Biophys. J.* 91 (2006) 1858–1867.
- [9] Q. Huai, H. Wang, Y. Sun, H.-Y. Kim, Y. Liu, H. Ke, Three-dimensional structures of PDE4D in complex with roliprams and implication on inhibitor selectivity, *Structure* 11 (2003) 865–873.
- [10] G.L. Card, B.P. England, Y. Suzuki, D. Fong, B. Powell, B. Lee, C. Luu, M. Tabrizid, S. Gillette, P.N. Ibrahim, D.R. Artis, G. Bollag, M.V. Milburn, S.-H. Kim, J. Schlessinger, K.Y.J. Zhang, Structural basis for the activity of drugs that inhibit phosphodiesterases, *Structure* 12 (2004) 2233–2247.
- [11] K.F. Rabe, Update on roflumilast, a phosphodiesterase 4 inhibitor for the treatment of chronic obstructive pulmonary disease, *Br. J. Pharmacol.* 163 (2011) 53–67.
- [12] Z.-Z. Zhou, B.-C. Ge, Y.-F. Chen, X.-D. Shi, X.-M. Yang, J.-P. Xu, Catecholic

- amides as potential selective phosphodiesterase 4D inhibitors: design, synthesis, pharmacological evaluation and structure–activity relationships, *Bioorg. Med. Chem.* 23 (2015) 7332–7339.
- [13] H. Wang, H. Robinson, H. Ke, The molecular basis for different recognition of substrates by phosphodiesterase families 4 and 10, *J. Mol. Biol.* 371 (2007) 302–307.
- [14] W. Huang, Y. Zhang, J.R. Sportsman, A fluorescence polarization assay for cyclic nucleotide phosphodiesterases, *J. Biomol. Screen.* 7 (2002) 215–222.
- [15] M.-Z. Zhang, Z.-Z. Zhou, X. Yuan, Y.-F. Cheng, B.-T. Bi, M.-F. Gong, Y.-P. Chen, J.-P. Xu, Chlorbipram: a novel PDE4 inhibitor with improved safety as a potential antidepressant and cognitive enhancer, *Eur. J. Pharmacol.* 721 (2013) 56–63.
- [16] M.J. Ashton, D.C. Cook, G. Fenton, J.A. Karlsson, M.N. Palfreyman, D. Raeburn, A.J. Ratcliffe, J.E. Souness, S. Thurairatnam, N. Vicker, Selective type IV phosphodiesterase inhibitors as antiasthmatic agents. The syntheses and biological activities of 3-(cyclopentyloxy)-4-methoxybenzamides and analogues, *J. Med. Chem.* 37 (1994) 1696–1703.
- [17] F.E. van Dooren, M.T. Schram, C.G. Schalkwijk, C.D. Stehouwer, R.M. Henry, P.C. Dagnelie, N.C. Schaper, C.J. van der Kallen, A. Koster, S.J. Sep, J. Denollet, F.R. Verhey, F. Pouwer, Associations of low grade inflammation and endothelial dysfunction with depression - the Maastricht Study, *Brain Behav. Immun.* 56 (2016) 390–396.
- [18] E. Boorman, Z. Zajkowska, R. Ahmed, C.M. Pariante, P.A. Zunszain, Crosstalk between endocannabinoid and immune systems: a potential dysregulation in depression? *Psychopharmacology* 233 (2016) 1591–1604.
- [19] K.W. Kelley, J.C. O'Connor, M.A. Lawson, R. Dantzer, S.L. Rodriguez-Zas, R.H. McCusker, Aging leads to prolonged duration of inflammation-induced depression-like behavior caused by *Bacillus Calmette-Guerin*, *Brain Behav. Immun.* 32 (2013) 63–69.
- [20] G. Sebastiani, C. Morissette, C. Lagace, M. Boule, M.-J. Ouellette, R.W. McLaughlin, D. Lacombe, F. Gervais, P. Tremblay, The cAMP-specific phosphodiesterase 4B mediates $A\beta$ -induced microglial activation, *Neurobiol. Aging* 27 (2006) 691–701.
- [21] A.N. Jain, Surflex-Dock 2.1: robust performance from ligand energetic modeling, ring flexibility, and knowledge-based search, *J. Comput. Aided. Mol. Des.* 21 (2007) 281–306.
- [22] A.N. Jain, Surflex: fully automatic flexible molecular docking using a molecular similarity-based search engine, *J. Med. Chem.* 46 (2003) 499–511.